Research in Pharmaceutical Sciences, June 2026; 21(3): 305-322
Received: 20-09-2025
Peer Reviewed: 11-10-2025
Revised: 29-11-2025
Accepted: 08-12-2025
Published: 10-05-2026

School of Pharmacy & Pharmaceutical Sciences
Isfahan University of Medical Sciences

Original Article

Thymoquinone and pentoxifylline modulate 5-fluorouracil-induced senescence and apoptosis in colorectal cancer spheroids

Fatemeh Makalani[1,2], Ali Ghanbari[3], Mohammad Reza Tabandeh[4,5], Touraj Zamir Nasta[3,6], Alborz Jafaei Souq[7], and Cyrus Jalili[3,*]

[1]Department of Anatomical Sciences, Kermanshah University of Medical Sciences, Kermanshah, I.R. Iran. [2]Student Research Committee, Kermanshah University of Medical Sciences, Kermanshah, I.R. Iran. [3]Medical Biology Research Center, Health Technology Institute, Kermanshah University of Medical Sciences, Kermanshah, I.R. Iran. [4]Department of Biochemistry and Molecular Biology, Faculty of Veterinary Medicine, Shahid Chamran University of Ahvaz, Ahvaz, I.R. Iran. [5]Stem Cells and Transgenic Technology Research Center, Shahid Chamran University of Ahvaz, Ahvaz, I.R. Iran. [6]Medicinal Plant Research Center, Ahvaz Judishapur University of Medical Sciences, Ahvaz, I.R. Iran. [7]School of Medicine, Abadan University of Medical Sciences, Abadan, Iran.

Abstract

Background and purpose: Targeting senescent tumor cells with senotherapeutic agents represents a novel therapeutic strategy in overcoming chemotherapy resistance during 5-fluorouracil (5-FU) treatment of colorectal cancer (CRC). This study aimed to evaluate the senotherapeutic potential of thymoquinone (TQ) and pentoxifylline (PTX) in a 3D spheroid model of CRC subjected to 5-FU-induced senescence.

Experimental approach: Caco-2 spheroids were generated *via* the hanging drop method on Poly-HEMA-coated plates with conditioned medium derived from HFF cells. Spheroids were treated for 24 h with 5-FU (60 µM; 50% of IC_{50}), TQ (30 µM; 50% of IC_{50}), and PTX (3.5 mM; 50% of IC_{50}). Cell viability was measured using the MTT assay. ROS and IL-8 levels were measured. Cell death and apoptosis were evaluated using Calcein-AM and Annexin V/PI assays, and western blotting was used to assess the expression of SASP and apoptosis-associated proteins. β-galactosidase activity was measured as a marker of senescence.

Findings/Results: 5-FU effectively induced senescence and apoptosis in Caco-2 spheroids, as evidenced by an increased expression of p53, p16, p21, and γ-H2AX, as well as an elevated secretion of ROS. Co-treatment with TQ and PTX acted as senotherapeutic agents by enhancing apoptotic cell death through modulation of Bax/Bcl2/cleaved caspase-3 and β-galactosidase activity, and by increasing oxidative stress. Notably, the combination of TQ and PTX was shown to support a greater senotherapeutic effect.

Conclusion and implications: Findings indicated that TQ and PTX acted as senotherapeutic agents in 5-FU-induced senescent CRC spheroids and may have potential as adjuvants to enhance CRC therapy.

Keywords: Apoptosis; Colorectal cancer; 5-Fluorouracil; Pentoxifylline; Senescence; Thymoquinone.

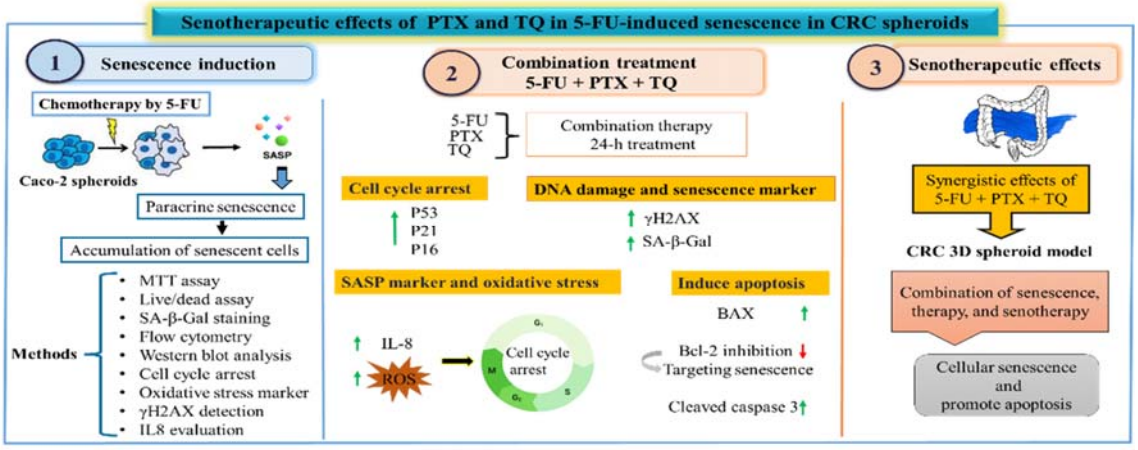

*Corresponding author: C. Jalili
Tel: +98-9188317220, Fax: +98-8334274622
Email: cjalili@kums.ac.ir

Access this article online
Website: http://rps.mui.ac.ir
DOI: 10.4103/RPS.RPS_175_25

INTRODUCTION

Colorectal cancer (CRC) is the third most common malignancy worldwide, and the second leading cause of cancer-related death, with an estimated 3.2 million new cases diagnosed by 2040, imposing a heavy burden on healthcare systems globally (1,2). The poor prognosis of CRC is largely attributed to resistance to chemotherapy and tumor recurrence (3).

Among current treatments, 5-fluorouracil (5-FU) remains the cornerstone chemotherapeutic drug for CRC. It functions as a thymidylate synthase inhibitor, thereby blocking thymidine synthesis and disrupting DNA replication in cancer cells (4,5). Anticancer therapies, including chemotherapy and radiotherapy, can induce a senescence-like state in cells, a phenomenon known as therapy-induced senescence (TIS). TIS has gained increasing scientific interest due to its role in cancer therapy, chemoresistance, and tumor recruitment (6). While senescence serves as a tumor-suppressive mechanism by affecting the proliferation of damaged cells, it also has a paradoxical role in cancer progression. Senescent tumor cells can secrete a variety of pro-inflammatory and pro-tumorigenic factors known as the senescence-associated secretory phenotype (SASP) (7). Cellular senescence is characterized by a stable cell-cycle arrest driven by activation of key regulators such as p16, p21, p27, and p53, together with the development of a SASP. Accumulation of therapy-induced senescent cells can promote tumor progression and resistance, which led to the emergence of "senotherapeutics" as a new strategy in cancer treatment. Senotherapeutic agents are broadly divided into two classes, including 1. senolytics, which selectively kill senescent cells (senolysis) and 2. senomorphics (or senostatics), which attenuate the pathological SASP and other harmful features of senescent cells without necessarily eliminating them (8-10).

Senolytic drugs reduce senescent cell viability by tipping the balance from stable arrest toward apoptosis, exploiting the dependence of senescent cells on pro-survival pathways. They target anti-apoptotic and survival signaling networks and thereby promote programmed cell death and clearance of senescent cells from tissues, potentially allowing replacement by healthy cells (11). In contrast, senomorphic agents do not remove senescent cells but reprogram their phenotype, particularly by suppressing SASP-driven chronic inflammation and metabolic stress. Senomorphic agents such as metformin, rapamycin, resveratrol, and curcumin act through transcriptional and signaling regulators such as NF-κB, JAK/STAT, mTOR, AMPK, and SIRT1 (12). Importantly, elevated p16/p21/p53 are widely used as markers of the senescent state, whereas senolytics are defined functionally by their ability to selectively eliminate senescent cells, and senomorphics by their capacity to blunt SASP and senescence-associated dysfunction (13,14). Several senolytic compounds, such as dasatinib, quercetin, and navitoclax, have been reported to enhance chemotherapy efficacy by targeting senescent cells through mechanisms including inhibition of anti-apoptotic proteins, disruption of survival signaling pathways, and modulation of the SASP. Current findings highlighted the combination of dasatinib and quercetin as an effective senolytic treatment, targeting and eliminating senescent cells. This combination induced apoptosis in senescent cells (15-17) .Despite advances in characterizing senescence in colorectal tumors, the development of effective senotherapeutic agents for resistant cells is still an active area of research. Therefore, an effective approach to enhance CRC therapy involves the combination of senotherapeutic compounds with chemotherapeutic drugs like 5-FU.

Thymoquinone (TQ), the bioactive ingredient found in black seed oil, exhibited anti-proliferative, antioxidant, anti-inflammatory, and apoptotic properties in several cancer cell lines (18,19). It has been reported that combination therapy with 5-FU, TQ, and coenzyme Q10 effectively modulated glycolysis and redox status in colon cancer cells (20). Specifically, the treatment led to a reduction in glycolytic activity, enhancement of oxidative stress, and promoted apoptosis in colon cancer cells by modulating the PI3K/AKT/mTOR pathway (21,22).

Pentoxifylline (7-Dimethyl-1-(5-oxohexyl) purine-2,6-dione; PTX) is a xanthine derivative and phosphodiesterase inhibitor commonly used to treat peripheral vascular disorders and is known to reduce the production of inflammatory cytokines (23,24). Furthermore, PTX induces caspase-dependent apoptosis in CRC cells through the mitochondrial pathway. The activation of Bax and Bid by PTX promoted mitochondrial outer membrane permeabilization, leading to the release of cytochrome c into the cytosol, activation of caspase-9 and caspase-3, triggering the apoptosis cascade (25,26). It has been demonstrated that 3D tumor models are more physiologically relevant and able to mimic tumor behaviors and characteristics compared to 2D models (27). 3D spheroid cell culture has emerged as a suitable tool for drug screening and drug toxicity. Spheroids are proposed as simple, compatible, robust, reproducible, and cost-effective models that can be used to mimic the complexity of *in vivo* tumors (28). Despite the known anticancer effects of TQ and PTX, their potential senotherapeutic effect, particularly their combination in the 3D spheroid model, remains underexplored. Monotherapy for cancer is often prone to drug resistance and tumor recurrence, which reduces the efficacy of the treatment (29). New approaches are required to enhance chemosensitivity. This study aimed to investigate the senotherapeutic effects of TQ and PTX against 5-FU-induced senescence in a 3D spheroid model of CRC.

MATERIALS AND METHODS

Cell line preparation and cell culture

Human colorectal adenocarcinoma cell line (Caco-2, HTB-37) and human foreskin fibroblasts (HFF, ATCC-SCRC-1041) were obtained from the Pasteur Institute (Tehran, Iran). Cells were cultured in high-glucose Dulbecco's modified Eagle's medium (HG-DMEM, Cat. No. BI-1003-1, Bioidea, Iran), supplemented with 10% fetal bovine serum (FBS, FB-1200, Biosera, France) and 1% antibiotics (100 IU/mL penicillin and 100 µg/mL streptomycin; Bioidea, BI-1203, Iran) in a humidified incubator (Padideh Nogene, Iran) with 37 °C temperature and 5% CO_2.

The cells were detached using 0.25% trypsin-EDTA (Bioidea, Iran) and incubated at 37 °C for 5 min until completely detached. The trypsinization was neutralized by adding complete growth medium, and the cell suspension was centrifuged at 1200 *g* for 10 min. The cell pellet was resuspended in fresh medium. Viable cells were counted using trypan blue (Sigma, USA).

This study was approved by the Research Ethics Committees of Medicine-Kermanshah University of Medical Sciences (Approval No. IR.KUMS.MED.REC.1402.062).

Preparation of HFF-conditioned media

HFF cells were cultivated in T25 flasks (Sanifico, South Korea) containing the complete medium (HG-DMEM supplemented with 10% FBS and 1% antibiotics) at a density of 0.5 × 10^6 cells for 3 days. Then, the supernatant was collected and centrifuged at 3000 *g* for 5 min to remove cell debris. The clarified supernatant was then filtered through a 0.22 µm pore size syringe filter (Biofil Co, India) to ensure sterility. The filtered HFF-1 conditioned medium was used immediately by mixing it at a 1:1 ratio with HG-DMEM culture medium for spheroid formation (30).

Preparation of Poly-HEMA-coated culture plates

Three-dimensional spheroids of Caco-2 cells were generated according to the protocols described previously, with a few modifications (31,32), using the hanging drop method on Poly (2-hydroxyethyl methacrylate) (Poly-HEMA)-coated plates. 1.2% Poly-HEMA solution was provided by dissolving 1.2 g of Poly-HEMA powder (Sigma-Aldrich, USA) in 100 mL of 95% ethanol, followed by overnight stirring. To prepare Poly-HEMA-coated plates, 50 µL of Poly-HEMA stock solution was added to each well of a 96-well U-bottom plate (Greiner BioOne, Austria).

Spheroid generation and evaluation

Caco-2 cells were detached from the flasks using the trypsin-EDTA solution and centrifuged at 2000 rpm for 10 min. The cell pellet was resuspended as a single-cell suspension at a density of 1 × 10^6 cells/mL at a

1:1 ratio of HG-DMEM and HFF1-derived medium. Next, 200 µL of this suspension was pipetted into each well of the Poly-HEMA-coated plate, followed by centrifugation at 220 *g* for 10 min. Plates were then incubated at 37 °C with 5% CO_2 to allow spheroid formation. Spheroid generation was evaluated for one week, using inverted microscopy (KoreaTech, South Korea). The morphology and diameter of the formed spheroids were examined by inverted light microscopy at days 0, 2, 5, and 7. Spheroid size was examined using Image J software (NIH, Bethesda, Maryland, USA) in 3 independent experiments with triplicate measurements. Spheroids with a diameter of approximately 150-200 µm with relatively smooth edges and a concentrated cell mass in the inner part were used for further experiments.

MTT assay and IC_{50} calculation

The toxicity of 5-FU (Cat No. F6627), PTX (Cat No. T7191), and TQ (Cat No. 274666) (Sigma-Aldrich, USA) against CRC spheroids was evaluated using 3-(4,5-Dimethylthiazol-2-yl)-2,5- diphenyltetrazolium bromide (MTT) assay. CRC spheroids were treated with TQ and 5-FU at the concentrations of 5,10, 20, 50, 100, 200, 400, and 800 µM and PTX at the concentrations of 1, 2, 4, 8, 16, 32, and 64 mM for 24 h. 100 µL of 0.5 mg/mL MTT solution (Cat No. M5655, Sigma Aldrich, USA) was added to each well, followed by incubating at 37 °C for 3 h. Then, the MTT solution was pulled out, and formazan crystals were dissolved in 100 µL of dimethyl sulfoxide (DMSO; Merck, Germany). The optical density (OD) was measured at 570 nm using a microplate reader (BioTek, USA). The analysis was conducted using three separate experiments. Cell viability was obtained using the following equation:

$$\text{Cell viability (\%)} = \frac{OD_T}{\text{OD}_C} \times 100$$

where, OD_T and OD_C expressed the OD for the treatment and the control groups, respectively.

Following the MTT assay, concentration-response curves were plotted in the GraphPad Prism software version 9 (GraphPad Software, San Diego, CA, USA), and IC_{50} values were determined.

Senescence induction and design of experimental groups

Twenty freshly formed Caco-2 spheroids were placed in 24-well plates containing HG-DMEM for each well. Then, spheroids were divided into 5 experimental groups as follows: 1. CRC spheroids without senescence induction (control); 2. 5-FU-induced senescent spheroids (5-FU); 3. 5-FU-induced senescent spheroids treated with the IC_{50} of PTX (5-FU + PTX); 4. 5-FU-induced senescent spheroids treated with the IC_{50} of TQ (5-FU + TQ); 5. 5-FU-induced senescent spheroids co-treated with the IC_{50} of PTX and TQ (5-FU + PTX + TQ).

Spheroids were first treated with 5-FU (60 µM; ~50% IC_{50}) for 48 h to induce senescence. Following senescence induction, spheroids were then treated simultaneously for an additional 24 h with 30 µM TQ (50% of IC_{50}) and 3.5 mM PTX (50% of IC_{50}).

Senescence-associated β-galactosidase assay

The senescence was determined by evaluation of β-galactosidase (β-gal) activity in experimental groups using the Senescence Detection Kit (Cat No. 9860, Cell Signaling Technology, USA), according to the manufacturer's instructions. After treatment, CRC spheroids were washed with phosphate-buffered saline (PBS) twice, fixed with 2% formaldehyde and 0.2% glutaraldehyde, and incubated in an X-gal staining solution overnight in the dark. After discarding the stain, samples were washed with PBS. Images of the stained spheroids were captured using a light microscope under the ×10 objective lens (Olympus BH-2, Japan) equipped with a digital Dino-Eye camera (AM7023, Taiwan) and Capture 2.0 software. For quantitative analysis, the intensity of the green-blue dye was assessed using ImageJ software. Untreated CRC spheroids and those treated with a known senescence inducer were assigned as the positive control. Negative control was considered spheroids treated with the staining solution without the addition of the X-gal substrate.

Apoptosis assay by Annexin V/propidium iodide assessment

To determine the apoptosis rate in treated spheroids, Annexin V-fluorescein isothiocyanate (FITC) and the propidium iodide (PI) detection kit (Padza, Iran) were used. Single-cell suspensions of spheroids were prepared using trypsin digestion. The cell suspension was then centrifuged at 1500 rpm for 5 min to pellet the cells, which were subsequently used for the apoptosis assay. The cells were washed twice with cold PBS and then resuspended in 1× binding buffer. The cells were stained for 15 min with Annexin V-FITC at room temperature in the dark. Afterward, PI was added, and the samples were analyzed by flow cytometer (BD Biosciences FACS Canto II, San Diego, CA, United States) within 15 min. FlowJo software version 10 (Tree Star Inc., USA) was used to analyze the results and calculate the distribution percentage of viable, early apoptotic, late apoptotic, and necrotic cells. The gating strategy included forward and side scatter to exclude debris, followed by Annexin V-FITC versus PI plots to define the four populations. The event count was set to a minimum of 10000 events per sample, and data were collected in triplicate for 3 independent experiments.

Live/dead cell staining

Spheroids were stained using a live/dead staining method as described previously (33). For each sample, 500 µL of the calcein acetoxymethyl (Calcein-AM) working solution (2 µM in PBS) and 50 µL of the PI (1 µg/mL in PBS) working solution were added to each well. The spheroids were then incubated with the staining solution at 37 °C for 1 min. After incubation, the spheroids were gently washed 2-3 times with PBS to remove excess dye. For imaging, the stained spheroids were transferred to a microscope slide and covered with a coverslip. The spheroids were visualized under a fluorescence microscope using appropriate filters; Calcein-AM (live cells) was visualized with excitation at 495 nm and emission at 515 nm (green fluorescence), while PI (dead cells) was visualized with excitation at 535 nm and emission at 617 nm (red fluorescence). The images were analysed using ImageJ software to quantify the populations of live and dead cells.

Western blot analysis

The expression of p53, P16, P21, Bcl2, Bax, cleaved caspase 3, and H2A histone family member X (H2AX) proteins in the treated spheroids was evaluated using the western blot method. The spheroids were lysed in 200 µL of lysis buffer (50 mM Tris-HCl, 150 mM NaCl, 0.1% Triton X-100, and 1 mM NaF) supplied with protease inhibitor cocktails (Sigma-Aldrich, MO, USA) for 30 min on ice. The protein concentration of the cell lysate was quantified using the Bradford protein assay. For electrophoresis, equal amounts (10 µg) of protein from each sample were denatured by adding 5× sodium dodecyl sulfate (SDS) sample buffer and incubating at 95 °C for 5 min. A total of 10 µg of protein per sample was loaded onto a 10% SDS-polyacrylamide gel electrophoresis (PAGE) and subjected to electrophoresis at 120 V for 2 h. The proteins were then transferred onto polyvinylidene fluoride (PVDF) membranes (Amersham, USA) and blocked overnight at 4 °C with 5% bovine serum albumin (BSA, Sigma, USA) in Tris-buffered saline (TBS, Sigma, USA) containing 0.05% Tween-20 (Sigma, USA), using a wet transfer system at 100 V for 1 h at 4 °C. The membrane was incubated with primary antibodies diluted 1:500 in blocking solution, as well as P53 (#2524), P16 (#80772), P21 (#2947), H2AX (#80312), Bcl2 (#4223), Bax (#2774), and caspase 3 (#9662) antibodies (Cell Signaling Technology, USA) for 2 h at room temperature. After 15-min-wash for 3 times in Tris-buffered saline with Tween 20, membranes were incubated with an appropriate secondary antibody (#96232, Cell Signaling Technology, USA) conjugated to horseradish peroxidase diluted 1:1000 in blocking solution for 2 h. Following 3 additional washes, protein reactivity was visualized using an electrochemiluminescence detection kit (ECL, Parstous, Iran). Protein loading was normalized to GAPDH immunoreactivity (D16H11; Cell Signaling Technology, USA). The blots were detected using the Fusion X chemiluminescence imaging system (Vilber, USA), and the results were expressed as fold change relative to the control group. Optical density analysis was performed using the Fusion X software and expressed as a fold change to the control group.

Detection of reactive oxygen species

The intracellular levels of reactive oxygen species (ROS) were measured using a ROS assay kit (KROS96, Kiazist, Iran) by using 2',7'-dichlorodihydrofluorescein diacetate (DCFDA), a non-fluorescent dye that interacts with ROS to create fluorescent 2,7-dichlorofluorescein (DCF). To determine the level of ROS in cells, the spheroids were dissociated and stained with 1 mM DCFDA solution in PBS and incubated in a 37 °C incubator for 30 min. Following the incubation, the cells were washed twice with 1× PBS and DCFDA, and fluorescence intensity was determined at 491 nm excitation and 516 nm emission using a fluorescence microplate reader (BipoTek Synergy H1, USA). The mean fluorescence intensity was normalized with blank media. Results were normalized by protein concentration assayed by the Bradford method and expressed relative to the control group.

Interleukin-8 assay

Interleukin-8 (IL-8) secretion was assessed using the ELISA kit (SL1736Hu, Sunlong Biotech, China). Supernatants of CRC spheroids were collected and centrifuged. Fifty µL of supernatants mixed with an equal volume of assay buffer (1×) were transferred to each well of the IL-8 microplate and incubated at room temperature for 1 h under mild shaking. Wells were washed with washing buffer (1.5×), 100 µL of substrate solution was added to each well, and the microplate was incubated at room temperature for 10 min in the dark. Then, 100 µL of stop solution was added to the wells, and OD values were measured at 450 nm in an ELISA reader (BioTek, USA). IL-8 levels were determined against a standard curve of IL-8 serial dilution and reported as pg/mg protein.

Statistical analysis

Quantitative data were obtained in triplicate. All data were reported as mean ± SD and analyzed using GraphPad Prism 9 software (GraphPad Software, San Diego, CA, USA). *P*-values < 0.05 were considered significant. The Shapiro-Wilk test was used to evaluate data normality or error variance equivalence. The data were analyzed using the one-way analysis of variance (ANOVA), followed by Tukey's test. For the synergy analysis, based on the highest single agent (HSA) model, the effect of the combination treatment was compared to the individual agent (PTX or TQ) using one-way ANOVA, followed by Tukey's test. A synergistic effect was identified if the combined treatment exhibited a significantly higher effect compared to the single agent.

RESULTS

Characteristics of CRC 3D spheroids from Caco-2 cells

After cultivating under sphere-forming conditions, Caco-2 cells were monitored daily regarding spheroid formation (Fig. 1). From day 2, spheroids appeared with visible aggregation of cells, while by day 5, spheroids exhibited a more compact and well-formed structure with a smooth edge. The cells were incubated for 7 days to achieve tight spheroid formation. By day 7, spheroids reached a diameter of approximately 150-200 µm, which was ideal for further experimental use.

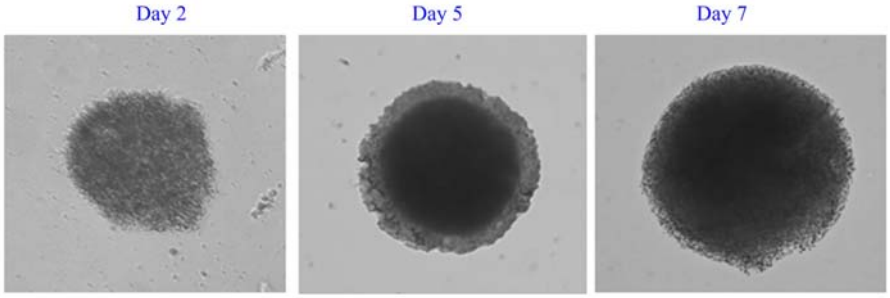

Fig. 1. Generation of Caco-2 3D spheroids using Poly-HEMA-coated plates and the fibroblast-conditioned medium. Images of morphology of CRC 3D spheroids from Caco-2 cells on days 2, 5, and 7 after culture were obtained using the inverted microscope (5×). On day 2, cells began to aggregate with loose and irregular boundaries; by day 5, the spheroid became more compact, with partial boundary smoothing; by day 7, a well-defined, dense, and nearly spherical structure with a smoother surface was observed, indicating maturation and stabilization of the spheroid architecture.

Effects of TQ and PTX on the cell viability of Caco-2 spheroids

The viability of Caco-2 spheroids treated with different doses of 5-FU, PTX, and TQ was evaluated using the MTT assay. The results showed that cell viability decreased in treated cells in a concentration-dependent manner, with remarkably reduced viability at higher concentrations. The IC_{50} values at 24 h, determined by the concentration-response curve, were 119.4 µM, 7.07 mM, and 58.34 µM for 5-FU, PTX, and TQ, respectively (Fig. 2).

Effect of TQ and PTX on the SA-β-Gal activity in Caco-2 spheroids

Senescence induction in spheroids treated with 5-FU, PTX, and TQ was assessed using β-Gal staining (Fig. 3A). The results demonstrated that 5-FU had a significant effect on SA-β-Gal activity compared to the control group. In the 5-FU + TQ and 5-FU + PTX + TQ groups, SA-β-Gal activity was significantly increased compared to the 5-FU group. However, no significant difference in senescence was observed between the 5-FU and 5-FU + PTX groups. The combination of PTX and TQ induced significantly higher SA-β-Gal activity compared to the individual treatments with PTX or TQ alone, indicating a synergistic effect of the combination on senescence induction (Fig. 3B).

Effect of TQ and PTX on apoptosis of Caco-2 spheroids

The rate of apoptosis of Caco-2-derived spheroids in different experimental groups is shown in Fig. 4. The apoptosis rate of Caco-2-derived spheroids was increased significantly in the 5-FU group compared with the control group. Notably, the combination of PTX and TQ significantly increased the apoptosis rate compared to the 5-FU and 5-FU + PTX groups, indicating a synergistic effect of the combination on senescence induction. The rate of apoptosis was significantly higher in the 5-FU + TQ group compared to the 5-FU and 5-FU + PTX groups (Fig. 4B).

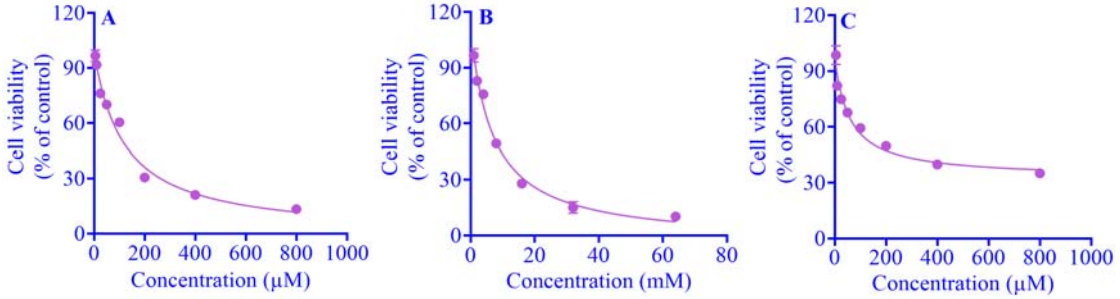

Fig. 2. Cytotoxic effects of (A) 5-FU, (B) PTX, and (C) TQ on Caco-2-derived spheroids. MTT assay was used to determine the IC_{50} values of 5-FU (119.4 µM), PTX (7.07 mM), and TQ (58.34 µM). For control, the cells were treated with 0.2% DMSO (vol/vol) in the cell culture media. Data were expressed as mean ± SD, n = 3. 5-FU, 5-Fluorouracil; PTX, pentoxifylline; TQ, thymoquinone.

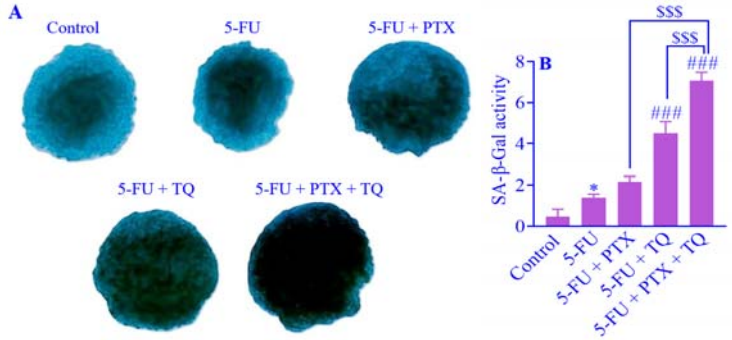

Fig. 3. The SA-β-Gal activity in Caco-2-derived spheroids following treatment with 5-FU (60 µM), PTX (3.5 mM), and TQ (30 µM) for 24 h. (A) Representative images and (B) graphs representing β-galactosidase-stained surface of spheroids. CRC spheroids without senescence induction were considered the control group. Data were expressed as mean ± SD, n = 3. $^{*}P < 0.05$ indicates significant difference compared to control group; $^{###}P < 0.001$ versus 5-FU group; $^{\$\$\$}P < 0.001$ represents the significant difference between the designated groups. 5-FU, 5-Fluorouracil; PTX, pentoxifylline; TQ, thymoquinone; SA-β-Gal, senescence-associated β-galactosidase.

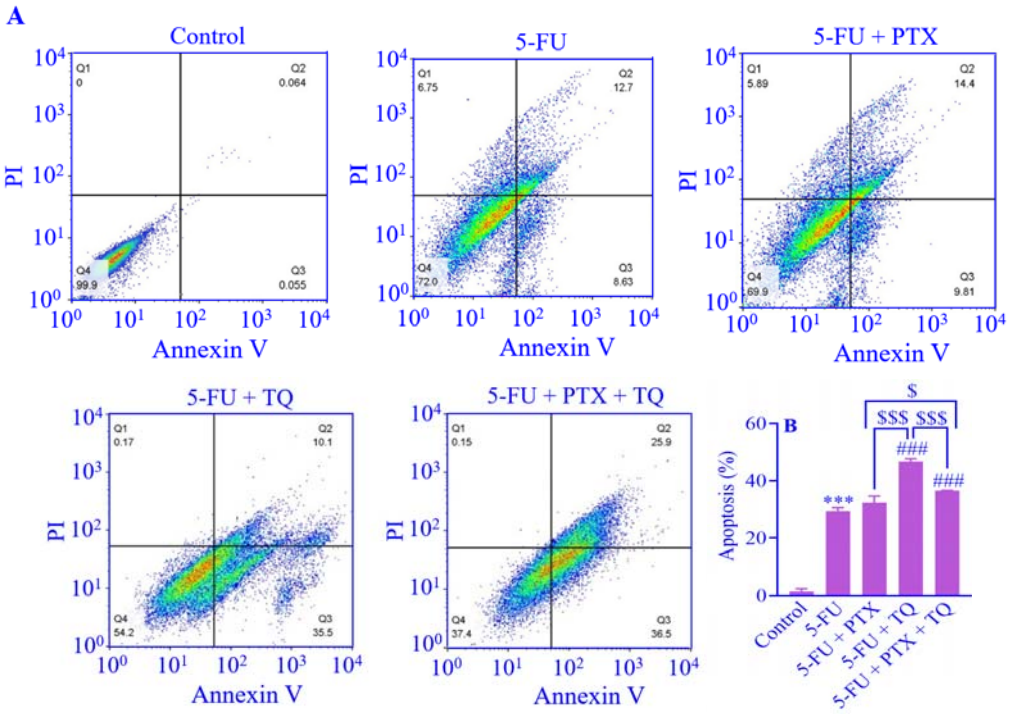

Fig. 4. Annexin V-FITC/PI staining of Caco-2-derived spheroids following treatment with 5-FU (60 µM), PTX (3.5 mM), and TQ (30 µM) for 24 h. CRC spheroids without senescence induction were considered the control group. (A) Flow cytometric analysis. The percentage of cells was shown for each quadrant. Data were presented as mean ± SD. Q1, Dead cells (AV-/PI+); Q2, late apoptotic cells (AV+ /PI+); Q3, early apoptotic cells (AV+ /PI-); Q4, live cells (AV-/PI-). (B) The percentage of apoptotic cells in Caco-2. Data were expressed as mean ± SD, n = 3. $^{***}P < 0.001$ indicates significant difference compared to the control group; $^{###}P < 0.001$ versus 5-FU group; $^{\$}P < 0.05$ and $^{\$\$\$}P < 0.001$ represent the significant differences between the designated groups. 5-FU, 5-Fluorouracil; PTX, pentoxifylline; TQ, thymoquinone; AV, Annexin V; PI, propidium iodide.

Effect of TQ and PTX on the viability of Caco-2 spheroids

The results of live/dead cell imaging of spheroids treated with 5-FU, TQ, and PTX, performed using Calcein-AM/PI staining to determine cell viability, are shown in Fig. 5. The mean relative fluorescence intensity of PI, a marker of dead cells, in Caco-2-derived spheroids was significantly increased in the 5-FU group compared to the control group. 5-FU treatment increased the number of red PI-positive cells in comparison to the control group, indicating enhanced cell death. In the 5-FU + TQ and 5-FU + PTX groups, mean relative fluorescence intensity of PI had no significant difference compared to the 5-FU group. Furthermore, the combination of TQ and PTX significantly resulted in a higher PI fluorescence intensity compared to the 5-FU, 5-FU + PTX, and 5-FU + TQ groups (Fig. 5).

Effect of TQ and PTX on the expression of cell cycle arrest and DNA damage associated with proteins in Caco-2 spheroids

Western blot analysis showed no significant change in p53 protein expression in the 5-FU group compared to the control group. Also, there was no significant change in the expression of p53 protein in the 5-FU + PTX and 5-FU + TQ groups compared to the 5-FU group. A significant increase was shown in the 5-FU + PTX + TQ group compared to the 5-FU + PTX and 5-FU + TQ groups (Fig. 6A) .The expression of p16 protein significantly increased in the 5-FU group compared to the control group. Also, a significant increase was seen in the expression of p16 protein in the 5-FU + PTX + TQ group compared to the 5-FU + PTX and 5-FU + TQ groups. The expression of p16 protein in the 5-FU + PTX group was significantly reduced compared to the 5-FU group. The p16 protein expression was significantly increased in the 5-FU + TQ group compared to the 5-FU + PTX (Fig. 6B).

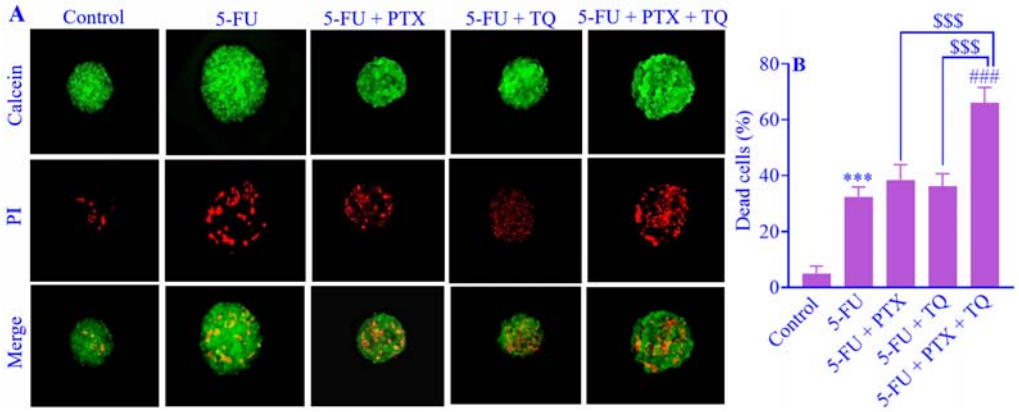

Fig. 5. Live/dead assay for the viability of the Caco-2-derived spheroids following treatment with 5-FU (60 µM), PTX (3.5 mM), and TQ (30 µM) for 24 h. CRC spheroids without senescence induction were considered the control group. (A) Quantification from the live/dead assay using ImageJ software. Green fluorescence indicates Calcein-AM stain in the live cells, and red fluorescence indicates the PI stain in the dead cells. (B**)** Mean relative fluorescence intensity of PI, a marker of dead cells. Data were expressed as mean ± SD, n = 3. $^{***}P < 0.001$ indicates significant difference compared to the control group; $^{\#\#\#}P < 0.001$ versus 5-FU group; $^{\$}P < 0.05$ and $^{\$\$\$}P < 0.001$ represent the significant differences between the designated groups. 5-FU, 5-Fluorouracil; PTX, pentoxifylline; TQ, thymoquinone; PI, propidium iodide.

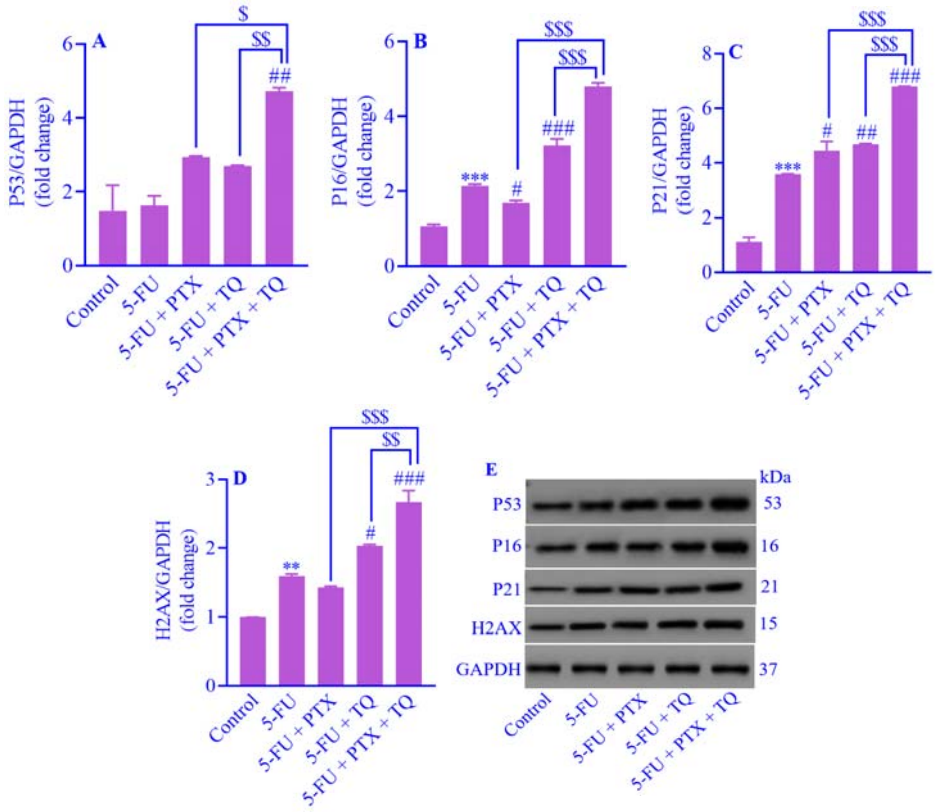

Fig. 6. The expression levels of (A) p53, (B) p16, (C) p21, and (D) H2AX proteins in Caco-2-derived spheroids following treatment with 5-FU (60 µM), PTX (3.5 mM), and TQ (30 µM) for 24 h using the western blot method. (E) Western blot images. CRC spheroids without senescence induction were considered the control group. GAPDH protein was used as a calibrator. Data were presented as mean ± SD, n = 2. $^{**}P < 0.01$ and $^{***}P < 0.001$ indicate significant differences compared to the control group; $^{\#}P < 0.05$, $^{\#\#}P < 0.01$, and $^{\#\#\#}P < 0.001$ versus 5-FU group; $^{\$}P < 0.05$, $^{\$\$}P < 0.01$, and $^{\$\$\$}P < 0.001$ represent the significant differences between the designated groups. 5-FU, 5-Fluorouracil; PTX, pentoxifylline; TQ, thymoquinone.

The expression of p21 protein was significantly increased in the 5-FU group compared to the control group. Moreover, the combination of PTX and TQ significantly enhanced the p21 expression compared to both the 5-FU + PTX and 5-FU + TQ groups (Fig. 6C).

H2AX protein expression was significantly increased in the 5-FU group compared to the control group. In addition, H2AX expression was significantly higher in the group treated with the PTX + TQ compared to the 5-FU + TQ and 5-FU + PTX groups. On the other hand, there was decreased H2AX expression in the 5-FU + PTX group compared to the 5-FU group, although this difference was not statistically significant. In contrast, the 5-FU + TQ group exhibited a significant increase in H2AX expression compared to the 5-FU group. Additionally, the 5-FU + PTX + TQ group showed a significant increase in H2AX expression compared to the group in which senescence was induced alone (Figs. 6D).

Western blot images of the protein relative expression are shown in Figs. 6E and S1.

Effect of TQ and PTX on the expression of apoptosis-associated proteins

The evaluation of Bax protein expression, a marker of apoptosis, showed an increase in the 5-FU group compared to the control group, although this increase was not statistically significant. The highest increase in Bax expression was observed in the 5-FU + PTX + TQ group, which showed a significant increase compared to the 5-FU + TQ, 5-FU + PTX, and 5-FU groups. Bax expression was significantly higher in the 5-FU + TQ group than both the 5-FU + PTX group and the 5-FU group, while no significant difference was observed between the 5-FU + PTX and 5-FU groups (Fig. 7A).

Bcl2 protein expression was decreased in the 5-FU group compared to the control group, but this difference was not significant. 5-FU + TQ and 5-FU + PTX groups showed a significant decrease in Bcl2 expression compared to the 5-FU group. Furthermore, the 5-FU + PTX group displayed a significant increase in Bcl2 expression compared to both the 5-FU + TQ and 5-FU + PTX + TQ groups (Fig. 7B)

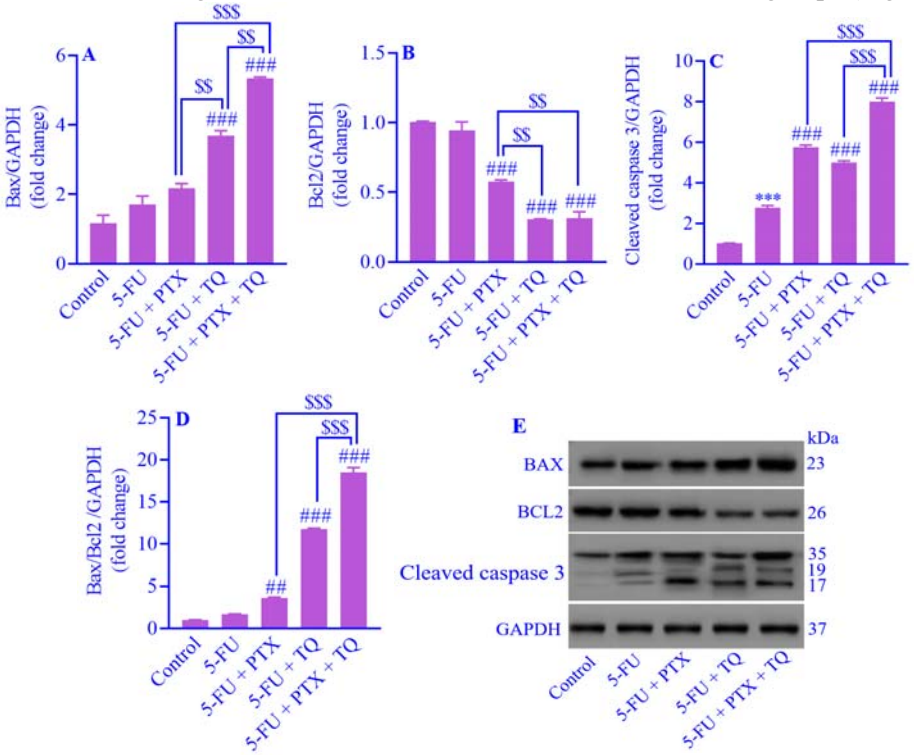

Fig. 7. The expression levels of (A) Bax, (B) Bcl2, and (C) cleaved caspase 3 proteins and (D) ratio of Bax/Bcl2 expression level in Caco-2 derived spheroids following treatment with 5-FU (60 µM), PTX (3.5 mM), and TQ (30 µM) for 24 h using the Western blot method. (E) Western blot images. CRC spheroids without senescence induction were considered the control group. GAPDH protein was used as a calibrator. Data were reported as mean ± SD, n = 2. $^{***}P < 0.001$ indicates significant difference compared to the control group; $^{\#\#}P < 0.01$ and $^{\#\#\#}P < 0.001$ versus 5-FU group; $^{\$\$}P < 0.01$ and $^{\$\$\$}P < 0.001$ represent the significant differences between the designated groups. 5-FU, 5-Fluorouracil; PTX, pentoxifylline; TQ, thymoquinone.

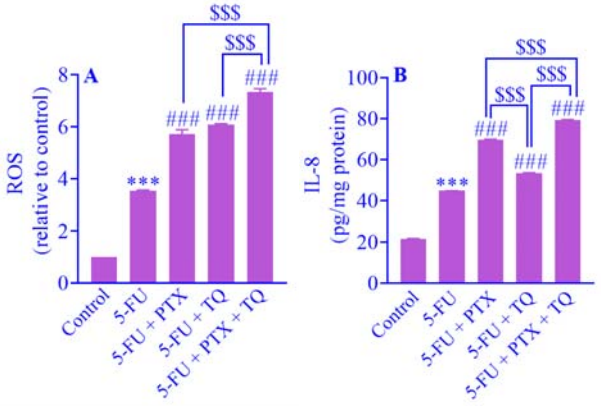

Fig. 8. The levels of (A) ROS and (B) IL-8 in Caco-2-derived spheroids following treatment with 5-FU (60 µM), PTX (3.5 mM), and TQ (30 µM) for 24 h. CRC spheroids without senescence induction were considered the control group. Data were presented as mean ± SD, n = 3. $^{***}P < 0.001$ indicates significant difference compared to the control group; $^{###}P < 0.001$ versus 5-FU group; $^{\$\$\$}P < 0.001$ represents the significant difference between the designated groups. 5-FU, 5-Fluorouracil; PTX, pentoxifylline; TQ, thymoquinone.

The expression of cleaved caspase 3 protein was significantly increased in 5-FU-treated cells compared to the control group. Additionally, the cleaved caspase 3 expression was significantly higher in the 5-FU + PTX, 5-FU + TQ, and 5-FU + PTX + TQ groups compared to the 5-FU group. The highest level of cleaved caspase 3 expression was observed in the 5-FU + PTX +TQ group (Fig. 7C).

The highest Bax/Bcl2 ratio was observed in the 5-FU + PTX + TQ group compared with other groups, significantly. Also, the Bax/Bcl2 ratio in the 5-FU + TQ and 5-FU + PTX groups displayed a significant increase compared to the 5-FU group (Figs. 7D).

Western blot images of the protein relative expression are shown in Figs. 7E and S1.

Effects of TQ and PTX on oxidative stress marker and IL-8 secretion in Caco-2 spheroids

The evaluation of ROS level as a marker of oxidative stress revealed a significant increase in ROS in the 5-FU group compared to the control group. A similar significant increase in ROS was observed in the 5-FU + TQ, 5-FU + PTX, and 5-FU + PTX + TQ groups, all of which were significantly higher compared to the 5-FU group. No significant difference in the ROS level was observed between the 5-FU + TQ and 5-FU + PTX groups. The highest increase in ROS level was observed in the 5-FU + PTX + TQ group, which showed a significant increase compared to the groups that received only PTX or TQ (Fig. 8A), indicating a synergistic effect of the combination of PTX and TQ.

The level of IL-8 was significantly elevated in all 5-FU-treated spheroids compared to the control group. The combination of PTX and TQ induced the highest increase in IL-8 level compared to other groups, significantly. Additionally, the 5-FU + PTX group showed a significantly higher level of IL-8 than the 5-FU + TQ group (Fig. 8B).

DISCUSSION

CRC remains a major clinical challenge globally due to its prevalence, high mortality, therapy resistance, and recurrence (34). Chemotherapy-induced senescence (CIS) is a double-edged sword: senescent cells secrete SASP factors that can promote tumor growth, metastasis, and relapse (35). Senolytics selectively eliminate senescent cells, reducing SASP-mediated inflammation and enhancing therapeutic efficacy (30). According to recent studies, piceatannol, hesperidin, and oleanolic acid are the most promising senolytic candidates for combating 5-FU-induced senescence, which could serve as adjuvant therapies to mitigate the adverse effects of chemotherapeutic senescence (36-38). Recent preclinical studies have indicated the benefits of senolytics in improving outcomes across various cancer models (39), however, their application in CRC, particularly within a 3D spheroid model, remains limited.

In this research, we investigated the senotherapeutic potential of TQ and PTX against 5-FU-induced senescence in CRC for the first time, using a 3D spheroid model that more closely mimics the *in vivo* tumor microenvironment.

The morphological features, size, and homogeneity of the spheroids observed in the present results were consistent with results in previous studies, successfully replicating a 3D colorectal tumor model (40,41). Poly-HEMA-coated plates prevented cell adhesion and enabled uniform spheroid formation, while fibroblast-conditioned medium enhanced spheroid maturation, simulating tumor-stroma interactions. This 3D model is reliable for evaluating therapies and, unlike 2D cultures, better reflects in vivo tumor complexity and heterogeneity (42). The present results demonstrated that 5-FU treatment induced significant senescence in Caco-2 colorectal spheroid cells, as evidenced by several markers of cellular stress and senescence.

Additionally, the results revealed an increase in senescence-associated β-Gal activity, a hallmark of senescence, further confirming the induction of senescence in response to 5-FU treatment. The current data also demonstrated significant upregulation of the tumor suppressor proteins p21, p16, and p53, which are key regulators of the senescence phenotype. Activation of these proteins leads to stable cell cycle arrest consistent with previous findings, indicating that DNA-damaging chemotherapeutics, such as 5-FU, promote senescence through the p16/p21/p53 pathway (43,44). Moreover, the increased γH2AX expression observed in this study suggested DNA damage response activation, which further supports the role of 5-FU in inducing cellular senescence *via* genotoxic stress (45,46). Interestingly, the ratio of Bax/Bcl2 remained unchanged in the 5-FU-treated Caco-2 spheroids, suggesting that while 5-FU induced senescence, it did not significantly alter the apoptotic balance in these cells. This result is in contrast to a study performed on endothelial cells, where 5-FU treatment led to significant shifts in the Bax/Bcl2 ratio, promoting apoptosis (47). However, the present findings are consistent with a previous study demonstrating that 5-FU induces cellular senescence together with either apoptosis or autophagy-mediated cell death in various cell types, suggesting context-dependent differences in cellular susceptibility to these pathways (48).

The increase in ROS production observed in this study is likely linked to mitochondrial dysfunction, a well-established driver of both oxidative stress and senescence. In line with this, mitochondrial ROS production and impaired mitophagy have been identified as key factors in 5-FU-induced senescence in other models, such as endothelial cells (49). This mitochondrial dysfunction can lead to metabolic alterations, including increased oxidative phosphorylation activity, even in the presence of inefficient electron transport and reduced ATP production, which may contribute to the persistence of the senescent state (50). While we did not observe changes in apoptosis markers such as the Bax/Bcl2 ratio, the induction of ROS, β-Gal activity, and the p16/p21/p53 axis in Caco-2 spheroids suggested a similar mechanism of CIS in CRC cells. These findings not only supported the dual role of 5-FU in inducing both senescence and apoptosis but also underscored the complex interplay between oxidative stress, mitochondrial dysfunction, and cellular fate mechanisms in response to chemotherapy.

PTX, a xanthine derivative, and TQ, a bioactive compound derived from *Nigella sativa*, have been known due to their anticancer properties (26,51), but their senotherapeutic effects in CRC were unclear. To assess this, 5-FU-induced senescent colorectal spheroids were treated with PTX and TQ individually and in combination. MTT assays showed that both agents significantly reduced cell viability, with the combination producing the most pronounced cytotoxic effect, indicating a synergistic interaction. Combination treatment with TQ and PTX significantly increased the pro-apoptotic protein Bax and decreased the anti-apoptotic protein Bcl2 compared to 5-FU and single treatments. This altered Bax/Bcl2 ratio promoted mitochondrial membrane permeability, cytochrome c release, and caspase activation, including elevated cleaved caspase 3, leading to apoptosis. Increased p53 expression further reflected activation of DNA damage response pathways and enhanced cell death.

Interestingly, p16 expression was significantly decreased in the PTX group compared to the 5-FU group, whereas treatment with TQ increased p16 levels. This differential regulation may reflect distinct effects on the maintenance of senescence (52). On one hand, PTX may partially reverse senescence-associated growth arrest and sensitize cells to apoptosis (53,54), while on the other hand, TQ may reinforce senescence signaling and facilitate apoptotic clearance (55). The reduction of p16 expression by PTX indicated a partial reversal or bypass of senescence and increased sensitivity of cells to apoptosis, which is consistent with studies showing that mitotic stress can overcome senescence barriers (56-58).

The Annexin V/PI assay indicated that the proportion of cells in early apoptosis was significantly higher in the PTX, TQ, and especially the combination of PTX and TQ groups compared to the 5-FU group. This suggests that both TQ and PTX possess potent pro-apoptotic activity capable of selectively eliminating senescent CRC cells induced by 5-FU. Senescent cells are metabolically active, growth-arrested and often resistant to apoptosis due to upregulation of anti-apoptotic pathways (8,59,60). The ability of TQ and PTX to overcome this resistance and trigger programmed cell death implied that these agents function as effective senotherapeutic agents. This aligns with previous findings, showing that compounds inducing mitotic stress or oxidative imbalance can sensitize senescent cells to undergo apoptosis (61,62).

The level of ROS in 5-FU-treated spheroids was significantly increased compared to the controls, and it was further elevated in the PTX-, TQ-, and PTX + TQ-treated groups. It has been shown that increased ROS can lead to oxidative DNA damage, enhance senescence, and stimulate apoptosis. TQ exerts its anticancer effects through the induction of oxidative stress, modulation of apoptotic proteins, and anti-inflammatory actions (55). The increase in ROS indicates that PTX and TQ enhance oxidative stress in senescent cells, contributing to increased apoptosis. The pro-oxidant effects of TQ in cancer cells have also been reported, potentially through mitochondrial disruption and NADPH oxidase activation (63). The synergic senotherapeutic effects of PTX and TQ likely arise from complementary mechanisms; PTX inhibits cell growth and apoptosis, while TQ amplifies oxidative stress and modulates inflammatory signaling (60,64).

IL-8 is a pro-inflammatory chemokine that promotes tumor proliferation, angiogenesis, and immune recruitment, contributing to a tumor-supportive microenvironment even during apoptosis (65). As a central SASP component, IL-8 plays a paradoxical role in therapy-induced senescence by both halting tumor growth and supporting a permissive microenvironment. In this study, 5-FU-treated spheroids showed elevated IL-8, consistent with a previous study, indicating increased SASP factors in senescent cells (66). Interestingly, the combination of PTX and TQ resulted in the highest level of IL-8, which suggests that these compounds may amplify the pro-inflammatory response during the early stages of senescence. This effect might reflect the context-dependent modulation of cytokine release during senescence induction and the early senolytic response (67,68). A similar finding observed in Bogdanova's study demonstrated that the combination of dasatinib and quercetin, as senolytic agents, increased the secretion of IL-6, another major pro-inflammatory cytokine in the SASP (30). This unexpected increase in IL-6 suggests that senolytic treatments, while effective in eliminating senescent cells, can paradoxically amplify SASP components like IL-6, thereby modulating the tumor microenvironment in complex ways. Similarly, Haubeiss *et al*. reported that dasatinib treatment upregulated IL-6 in a CAF model, further supporting the idea that senolytic therapies may provoke a transient pro-inflammatory response (69). Moreover, Du *et al*. investigated cisplatin-induced senescence and found that senolytic therapy with dasatinib/quercetin resulted in increased secretion of IL-1β (70). Further research is needed to investigate the precise molecular mechanisms through which PTX and TQ modulate IL-8 and other SASP factors, and how these factors contribute to the senotherapeutic effects observed in the treatment groups. Additionally, longer-term time points

and dose-response studies will be essential in assessing the temporal dynamics of IL-8 secretion and other inflammatory markers, as well as the overall impact on tumor progression.

The SA-β-Gal assay revealed a significant increase in 5-FU-induced senescent spheroids compared to the control, confirming effective senescence induction in the 3D CRC model. Treatment with TQ and PTX, individually or combined, further elevated β-Gal activity, with the combination showing the highest level, suggesting a synergistic effect.

Although senolytic agents are typically expected to reduce SA-β-Gal activity by eliminating senescent cells, the current research exhibited that this activity was unexpectedly elevated after treatment with TQ and PTX, especially in combination. These findings suggest that TQ and PTX may not behave as classical senolytics under the conditions tested, but rather as senotherapeutic agents that remodel senescence pathways in CRC cells. In line with this, the present findings revealed increased expression of cell-cycle inhibitors (p21, p16, and p53) together with modulation of SASP-related and apoptotic markers, indicating reinforcement of senescence and activation of stress and death pathways rather than simple depletion of the senescent population. Given that cancer cells often exhibit rewired senescence and survival signaling, it is plausible that TQ and PTX shift the balance toward a more stable, growth-arrested, and pro-apoptotic state without immediately reducing the pool of SA-β-Gal-positive cells. Therefore, on the basis of present data, these compounds are better described as senotherapeutic agents modulating senescence and apoptosis in 5-FU-treated CRC spheroids, rather than routine senolytics, while their potential senolytic effects may be context- and time-dependent and warrant further investigation.

The current study findings may also be explained by alternative mechanisms. Firstly, TQ and PTX are known to induce oxidative stress, which can lead to a senescence-like response in cells. In this early phase, cells may exhibit increased β-Gal activity as a stress marker before progressing to actual cell death. This phenomenon is consistent with the SASP, a hallmark of senescence, where the secretion of pro-inflammatory cytokines and other factors occurs, potentially increasing β-Gal activity as part of the early senescence response. Secondly, both TQ and PTX may induce senescence in precursor cells that are not fully senescent but are on the brink of entering a senescent state. These precursor cells may exhibit a transient increase in β-Gal activity, which could reflect an early-stage senescence marker before the cells fully undergo senolysis. The elevated β-Gal activity in these cells would thus represent a temporary response to oxidative stress or SASP induction rather than a stable feature of fully senescent cells. Taken together, these findings suggest that the combination of TQ and PTX may lead to biphasic effects. Initially, they may induce a senescence-like phenotype, including elevated β-Gal activity. Over time, these agents may trigger senolysis, the ultimate removal of these senescent cells *via* apoptosis. Therefore, the observed increase in β-Gal activity could be part of an early senescence phase, which precedes the apoptotic elimination of these cells (71-73).

CONCLUSION

The present study showed that TQ and PTX enhanced senotherapy activity in 5-FU-induced senescent CRC spheroids by modulating the senescence-associated secretory phenotype and activating apoptotic pathways. The combination of TQ and PTX, through ROS-mediated mechanisms, sensitized cells to 5-FU, improving its therapeutic efficiency. In a 3D spheroid model, the co-treatment effectively modulated senescence and promoted apoptosis, indicating a promising strategy to improve CRC therapy and reduce recurrence.

Acknowledgments

This work, as part of a Ph.D. project, was financially supported by the Research Deputy of Kermanshah University of Medical Sciences through Grant No. 4020253. The authors also acknowledge Avin Stem Gen Bio Health Inc. for providing technical support and assisting with parts of the laboratory procedures.

Conflict of interest statement

The authors declared no conflict of interest in this study.

Authors' contributions

F. Makalani developed the hypothesis and performed the literature search; A. Ghanbari, T. Zamir Nasta, and A. Jafaei Souq contributed to the design and conceptualization of the study; F. Makalani, M.R. Tabandeh, and C. Jalili analyzed the data and wrote the manuscript; C. Jalili carried out a thorough editing of the text.

All authors have read and approved the finalized article. Each author has fulfilled the authorship criteria and affirmed that this article represents honest and original work.

AI declaration

The authors did not use any AI-assisted technologies in the preparation of this manuscript.

REFERENCES

1. Bray F, Laversanne M, Sung H, Ferlay J, Siegel RL, Soerjomataram I, *et al*. Global cancer statistics 2022: GLOBOCAN estimates of incidence and mortality worldwide for 36 cancers in 185 countries. CA Cancer J Clin. 2024;74(3):229-263. DOI: 10.3322/caac.21834.
2. Morgan E, Arnold M, Gini A, Lorenzoni V, Cabasag CJ, Laversanne M, *et al*. Global burden of colorectal cancer in 2020 and 2040: incidence and mortality estimates from GLOBOCAN. Gut. 2023;72(2):338-344. DOI: 10.1136/gutjnl-2022-327736.
3. Elbadawy M, Usui T, Yamawaki H, Sasaki K. Development of an experimental model for analyzing drug resistance in colorectal cancer. Cancers (Basel). 2018;10(6):164,1-7. DOI: 10.3390/cancers10060164.
4. He S, Wang Z, Xia J, Jia H, Dai Q, Chen C, *et al*. Dasabuvir alleviates 5-fluorouracil-induced intestinal injury through anti-senescence and anti-inflammatory. Sci Rep. 2024;14(1):15730,1-13. DOI: 10.1038/s41598-024-66771-x.
5. Mohammadian M, Zeynali S, Fathi Azarbaijani A, Khadem Ansari MH, Kheradmand F. Cytotoxic effects of the newly-developed chemotherapeutic agents 17-AAG in combination with oxaliplatin and capecitabine in colorectal cancer cell lines. Res Pharm Sci. 2017;12(6):517-525. DOI: 10.4103/1735-5362.217432.
6. Wang B, Kohli J, Demaria M. Senescent cells in cancer therapy: friends or foes? Trends Cancer. 2020;6(10):838-857. DOI: 10.1016/j.trecan.2020.05.004.
7. Farfariello V, Gordienko DV, Mesilmany L, Touil Y, Germain E, Fliniaux I, *et al*. TRPC3 shapes the ER-mitochondria Ca^{2+} transfer, characterizing tumour-promoting senescence. Nat Commun. 2022;13(1):956,1-18. DOI: 10.1038/s41467-022-28597-x.
8. Hu L, Li H, Zi M, Li W, Liu J, Yang Y, *et al*. Why senescent cells are resistant to apoptosis: an insight for senolytic development. Front Cell Dev Biol. 2022;10:822816,1-17. DOI: 10.3389/fcell.2022.822816.
9. Dong Z, Luo Y, Yuan Z, Tian Y, Jin T, Xu F. Cellular senescence and SASP in tumor progression and therapeutic opportunities. Mol Cancer. 2024;23(1):181,1-19. DOI: 10.1186/s12943-024-02096-7.
10. Calcinotto A, Kohli J, Zagato E, Pellegrini L, Demaria M, Alimonti A. Cellular senescence: aging, cancer, and injury. Physiol Rev. 2019;99(2):1047-1078. DOI: 10.1152/physrev.00020.2018.
11. Miller SJ, Darji RY, Walaieh S, Lewis JA, Logan R. Senolytic and senomorphic secondary metabolites as therapeutic agents in *Drosophila melanogaster* models of Parkinson's disease. Front Neurol. 2023;14:1271941,1-19. DOI: 10.3389/fneur.2023.1271941.
12. Alum EU, Izah SC, Uti DE, Ugwu OPC, Betiang PA, Basajja M, *et al*. Targeting cellular senescence for healthy aging: advances in senolytics and senomorphics. Drug Des Devel Ther. 2025;19:8489-8522. DOI: 10.2147/DDDT.S543211.
13. Liang Y, Wang M, Wang X, Yang Z, Wang S, Li F, *et al*. Cellular senescence in colorectal cancer: its occurrence, effect and therapy. Front Oncol. 2025;15:1580951,1-18. DOI: 10.3389/fonc.2025.1580951.
14. Di Micco R, Krizhanovsky V, Baker D, d'Adda di Fagagna F. Cellular senescence in ageing: from mechanisms to therapeutic opportunities. Nat Rev Mol Cell Biol. 2021;22(2):75-95. DOI: 10.1038/s41580-020-00314-w.
15. Malavolta M, Pierpaoli E, Giacconi R, Costarelli L, Piacenza F, Basso A, *et al*. Pleiotropic effects of tocotrienols and quercetin on cellular senescence: introducing the perspective of senolytic effects of phytochemicals. Curr Drug Targets. 2016;17(4):447-459. DOI: 10.2174/1389450116666150907105104.
16. Zhang N, Gao M, Wang Z, Zhang J, Cui W, Li J, *et al*. Curcumin reverses doxorubicin resistance in colon cancer cells at the metabolic level. J Pharm Biomed Anal. 2021;201:114129. DOI: 10.1016/j.jpba.2021.114129.
17. Liu X, Wang Y, Zhang X, Gao Z, Zhang S, Shi P, *et al*. Senolytic activity of piperlongumine analogues: synthesis and biological evaluation. Bioorg Med Chem. 2018;26(14):3925-3938. DOI: 10.1016/j.bmc.2018.06.013.
18. Banerjee S, Padhye S, Azmi A, Wang Z, Philip PA, Kucuk O, *et al*. Review on molecular and therapeutic potential of thymoquinone in cancer. Nutr Cancer. 2010;62(7):938-946. DOI: 10.1080/01635581.2010.509832.
19. Mahmoud YK, Abdelrazek HMA. Cancer: Thymoquinone antioxidant/pro-oxidant effect as potential anticancer remedy. Biomed Pharmacother. 2019;115:108783,1-14. DOI: 10.1016/j.biopha.2019.108783.

20. Aslam A, Minshawi F, Almasmoum H, Almaimani R, Alsaegh A, Mahbub AA, *et al*. Exploring potential additive effects of 5-fluorouracil, thymoquinone, and coenzyme Q10 triple therapy on colon cancer cells in relation to glycolysis and redox status modulation. J Egypt Natl Canc Inst. 2025;37(1):7. DOI: 10.1186/s43046-025-00261-7.
21. Kurowska N, Madej M, Strzalka-Mrozik B. Thymoquinone: a promising therapeutic agent for the treatment of colorectal cancer. Curr Issues Mol Biol. 2023;46(1):121-139. DOI: 10.3390/cimb46010010.
22. Lei X, Lv X, Liu M, Yang Z, Ji M, Guo X, *et al*. Thymoquinone inhibits growth and augments 5-fluorouracil-induced apoptosis in gastric cancer cells both *in vitro* and *in vivo*. Biochem Biophys Res Commun. 2012;417(2):864-868. DOI: 10.1016/j.bbrc.2011.12.063.
23. Fernandes JL, de Oliveira RTD, Mamoni RL, Coelho OR, Nicolau JC, Blotta MHSL, *et al*. Pentoxifylline reduces pro-inflammatory and increases anti-inflammatory activity in patients with coronary artery disease--a randomized placebo-controlled study. Atherosclerosis. 2008;196(1):434-442. DOI: 10.1016/j.atherosclerosis.2006.11.032.
24. Rieneck K, Diamant M, Haahr PM, Schönharting M, Bendtzen K. *In vitro* immunomodulatory effects of pentoxifylline. Immunol Lett. 1993;37(2-3):131-138. DOI: 10.1016/0165-2478(93)90022-t.
25. Shirakami Y, Kochi T, Kubota M, Sakai H, Ibuka T, Yoshimi K, *et al*. Inhibitory effects of pentoxifylline on inflammation-related tumorigenesis in rat colon. Oncotarget. 2018;9(74):33972-33981. DOI: 10.18632/oncotarget.26119.
26. Al-Husein BA, Mhaidat NM, Alzoubi KH, Alzoubi GM, Alqudah MAY, Albsoul-Younes AM, *et al*. Pentoxifylline induces caspase-dependent apoptosis in colorectal cancer cells. Inform Med Unlocked. 2022;31:100997,1-6. DOI: 10.1016/j.imu.2022.100997.
27. Breslin S, O'Driscoll L. Three-dimensional cell culture: the missing link in drug discovery. Drug Discov Today. 2013;18(5-6):240-249. DOI: 10.1016/j.drudis.2012.10.003.
28. Arora S, Singh S, Mittal A, Desai N, Khatri DK, Gugulothu D, et al. Spheroids in cancer research: recent advances and opportunities. J Drug Deliv Sci Technol. 2024;100:106033. DOI: 10.1016/j.jddst.2024.106033.
29. Khajeh E, Rasmi Y, Kheradmand F, Malekinejad H, Aramwit P, Saboory E, *et al*. Crocetin suppresses the growth and migration in HCT-116 human colorectal cancer cells by activating the p-38 MAPK signaling pathway. Res Pharm Sci. 2020;15(6):592-601. DOI: 10.4103/1735-5362.301344.
30. Bogdanova DA, Kolosova ED, Pukhalskaia TV, Levchuk KA, Demidov ON, Belotserkovskaya EV. The differential effect of senolytics on SASP cytokine secretion and regulation of EMT by CAFs. Int J Mol Sci. 2024;25(7):4031. DOI: 10.3390/ijms25074031.
31. Phung YT, Barbone D, Broaddus VC, Ho M. Rapid generation of *in vitro* multicellular spheroids for the study of monoclonal antibody therapy. J Cancer. 2011;2:507-514. DOI: 10.7150/jca.2.507.
32. Al Hrout A, Cervantes-Gracia K, Chahwan R, Amin A. Modelling liver cancer microenvironment using a novel 3D culture system. Sci Rep. 2022;12(1):8003,1-14. DOI: 10.1038/s41598-022-11641-7.
33. Phour J, Vassella E. Methods in cancer research: assessing therapy response of spheroid cultures by life cell imaging using a cost-effective live-dead staining protocol. Biol Methods Protoc. 2024;9(1):bpae060,1-5. DOI: 10.1093/biomethods/bpae060.
34. Rawla P, Sunkara T, Barsouk A. Epidemiology of colorectal cancer: incidence, mortality, survival, and risk factors. Prz Gastroenterol. 2019;14(2):89-103. DOI: 10.5114/pg.2018.81072.
35. Guillon J, Petit C, Toutain B, Guette C, Lelièvre E, Coqueret O. Chemotherapy-induced senescence, an adaptive mechanism driving resistance and tumor heterogeneity. Cell cycle. 2019;18(19):2385-2397. DOI: 10.1080/15384101.2019.1652047.
36. Ambrosino A, Patrone D, Moriello C, Al-Sammarraie SHA, Lettiero I, Finicelli M, *et al*. Selective senolysis of 5FU-induced CRC senescent cells by piceatannol through mitochondrial depolarization and AIF-dependent apoptosis. Int J Mol Sci. 2025;26(18):9134,1-13. DOI: 10.3390/ijms26189134.
37. Iswarya BR, John CM. Modulating senescence-associated secretory phenotype-driven paracrine effects to overcome therapy -induced senescence: senolytic effects of hesperidin and quercetin in A549 lung adenocarcinoma cells. Mol Biol Rep. 2025;52(1):795. DOI: 10.1007/s11033-025-10904-6.
38. Bai SR, Zhao BX, Zhao Q, Ge YC, Li M, Zhao CG, *et al*. Oleanolic acid improves 5-fluorouracil-induced intestinal damage and inflammation by alleviating intestinal senescence. Sci Rep. 2024;14(1): 21852,1-15. DOI: 10.1038/s41598-024-72536-3.
39. Li W, Qin L, Feng R, Hu G, Sun H, He Y, Zhang R. Emerging senolytic agents derived from natural products. Mech of Ageing Dev.2019; Jul; 181:1-6. DOI:10.1016/j.mad.2019.05.001.
40. Gheytanchi E, Naseri M, Karimi-Busheri F, Atyabi F, Mirsharif ES, Bozorgmehr M, *et al*. Morphological and molecular characteristics of spheroid formation in HT-29 and Caco-2 colorectal cancer cell lines. Cancer Cell Int. 2021;21(1):204,1-16. DOI: 10.1186/s12935-021-01898-9.
41. Abbas ZN, Al-Saffar AZ, Jasim SM, Sulaiman GM. Comparative analysis between 2D and 3D colorectal cancer culture models for insights into cellular morphological and transcriptomic variations. Sci Rep. 2023;13(1):18380,1-16. DOI: 10.1038/s41598-023-45144-w.

42. Thakuri PS, Liu C, Luker GD, Tavana H. Biomaterials-based approaches to tumor spheroid and organoid modeling. Adv Healthc Mater. 2018;7(6):e1700980,1-42. DOI: 10.1002/adhm.201700980.
43. Maiuthed A, Ninsontia C, Erlenbach-Wuensch K, Ndreshkjana B, Muenzner JK, Caliskan A, *et al*. Cytoplasmic p21 mediates 5-fluorouracil resistance by inhibiting pro-apoptotic Chk2. Cancers (Basel). 2018;10(10):373,1-22. DOI: 10.3390/cancers10100373.
44. Cho YH, Ro EJ, Yoon JS, Mizutani T, Kang DW, Park JC, *et al*. 5-FU promotes stemness of colorectal cancer *via* p53-mediated WNT/β-catenin pathway activation. Nat Commun. 2020;11(1):5321,1-13. DOI: 10.1038/s41467-020-19173-2.
45. Adamsen BL, Kravik KL, De Angelis PM. DNA damage signaling in response to 5-fluorouracil in three colorectal cancer cell lines with different mismatch repair and TP53 status. Int J Oncol. 2011;39(3):673-682. DOI: 10.3892/ijo.2011.1080.
46. Ludikhuize MC, Gevers S, Nguyen NTB, Meerlo M, Roudbari SKS, Gulersonmez MC, *et al*. Rewiring glucose metabolism improves 5-FU efficacy in p53-deficient/KRAS^{G12D} glycolytic colorectal tumors. Commun Biol. 2022;5(1):1159,1-16. DOI: 10.1038/s42003-022-04055-8.
47. Altieri P, Murialdo R, Barisione C, Lazzarini E, Garibaldi S, Fabbi P, *et al*. 5-fluorouracil causes endothelial cell senescence: potential protective role of glucagon-like peptide 1. Br J Pharmacol. 2017;174(21):3713-3726. DOI: 10.1111/bph.13725.
48. Milczarek M, Wiktorska K, Mielczarek L, Koronkiewicz M, Dąbrowska A, Lubelska K, *et al*. Autophagic cell death and premature senescence: new mechanism of 5-fluorouracil and sulforaphane synergistic anticancer effect in MDA-MB-231 triple negative breast cancer cell line. Food Chem Toxicol. 2018;111:1-8. DOI: 10.1016/j.fct.2017.10.056.
49. Focaccetti C, Bruno A, Magnani E, Bartolini D, Principi E, Dallaglio K, *et al*. Effects of 5-fluorouracil on morphology, cell cycle, proliferation, apoptosis, autophagy and ROS production in endothelial cells and cardiomyocytes. PLoS One. 2015;10(2):e0115686,1-25. DOI: 10.1371/journal.pone.0115686.
50. Miwa S, Kashyap S, Chini E, von Zglinicki T. Mitochondrial dysfunction in cell senescence and aging. J Clin Invest. 2022;132(13):e158447,1-9. DOI: 10.1172/JCI158447.
51. Sheikhnia F, Rashidi V, Maghsoudi H, Majidinia M. Potential anticancer properties and mechanisms of thymoquinone in colorectal cancer. Cancer Cell Int. 2023;23(1):320,1-15. DOI: 10.1186/s12935-023-03174-4.
52. Muss HB, Smitherman A, Wood WA, Nyrop K, Tuchman S, Randhawa PK, *et al*. p16 a biomarker of aging and tolerance for cancer therapy. Transl Cancer Res. 2020;9(9):5732-5742. DOI: 10.21037/tcr.2020.03.39.
53. Kumar A, Rajput DS, Gupta MK, Kumar V, Singh H, Mishra AK, *et al*. A novel phosphodiesterase target as a therapeutic approach: inhibiting DEN-induced hepatocellular carcinoma progression. EXCLI J. 2025;24:407-429. DOI: 10.17179/excli2024-7941.
54. Rauko P, Sedlák J, Duraj J, Szekeres MF, Novotný L. Pentoxifylline stimulates drug-induced apoptosis in leukemic cells. Neoplasma. 1998;45(5):296-300. PMID: 9921918.
55. Abd El-Ghany RM, Sharaf NM, Kassem LA, Mahran LG, Heikal OA. Thymoquinone triggers anti-apoptotic signaling targeting death ligand and apoptotic regulators in a model of hepatic ischemia reperfusion injury. Drug Discov Ther. 2009;3(6):296-306. PMID: 22495664.
56. Buj R, Leon KE, Anguelov MA, Aird KM. Suppression of p16 alleviates the senescence-associated secretory phenotype. Aging (Albany NY). 2021;13(3):3290-3312. DOI: 10.18632/aging.202640.
57. Prime SS, Cirillo N, Parkinson EK. Escape from cellular senescence is associated with chromosomal instability in oral pre-malignancy. Biology (Basel). 2023;12(1):103,1-19. DOI: 10.3390/biology12010103.
58. Demidenko ZN, Blagosklonny MV. Growth stimulation leads to cellular senescence when the cell cycle is blocked. Cell Cycle. 2008;7(21):3355-3361. DOI: 10.4161/cc.7.21.6919.
59. Golunski G, Woziwodzka A, Piosik J. Potential use of pentoxifylline in cancer therapy. Curr Pharm Biotechnol. 2018;19(3):206-216. DOI: 10.2174/1389201019666180528084641.
60. Cerda-Cruz CR, Vazquez-Urrutia JR, Ortiz-Lazareno PC, Villaseñor-García MM, Cruz-Lozano JR, Hernández-Flores G, et al. Chemotherapy with a molecular rational basis, pentoxifylline as a promising antitumor drug. Ann Med Surg (Lond). 2025;87(3):1506-1528. DOI: 10.1097/MS9.0000000000003043.
61. Kracikova M, Akiri G, George A, Sachidanandam R, Aaronson SA. A threshold mechanism mediates p53 cell fate decision between growth arrest and apoptosis. Cell Death Differ. 2013;20(4):576-588. DOI: 10.1038/cdd.2012.155.
62. Yosef R, Pilpel N, Tokarsky-Amiel R, Biran A, Ovadya Y, Cohen S, *et al*. Directed elimination of senescent cells by inhibition of BCL-W and BCL-XL. Nat Commun. 2016;7:11190,1-11. DOI: 10.1038/ncomms11190.
63. Adinew GM, Messeha SS, Taka E, Badisa RB, Soliman KFA. Anticancer effects of thymoquinone through the antioxidant activity, upregulation of Nrf2, and downregulation of PD-L1 in triple-negative breast cancer cells. Nutrients. 2022;14(22):4787,1-25. DOI: 10.3390/nu14224787.
64. Majdalawieh AF, Al-Samaraie S, Terro TM. Molecular mechanisms and signaling pathways underlying the therapeutic potential of thymoquinone against colorectal cancer. Molecules. 2024;29(24):5907,1-15. DOI: 10.3390/molecules29245907.

65. Meier C, Brieger A. The role of IL-8 in cancer development and its impact on immunotherapy resistance. Eur J Cancer. 2025;218:115267. DOI: 10.1016/j.ejca.2025.115267.
66. Ortiz-Montero P, Londoño-Vallejo A, Vernot JP. Senescence-associated IL-6 and IL-8 cytokines induce a self- and cross-reinforced senescence/inflammatory milieu, strengthening tumorigenic capabilities in the MCF-7 breast cancer cell line. Cell Commun Signal. 2017;15(1):17,1-18. DOI: 10.1186/s12964-017-0172-3.
67. Saliev T, Singh PB. Targeting senescence: a review of senolytics and senomorphics in anti-aging interventions. Biomolecules. 2025;15(6):860,1-19. DOI: 10.3390/biom15060860.
68. Neuner P, Klosner G, Schauer E, Pourmojib M, Macheiner W, Grünwald C, *et al*. Pentoxifylline *in vivo* down-regulates the release of IL-1 beta, IL-6, IL-8 and tumour necrosis factor-alpha by human peripheral blood mononuclear cells. Immunology. 1994;83(2):262-267. PMID: 7835945.
69. Haubeiss S, Schmid JO, Mürdter TE, Sonnenberg M, Friedel G, van der Kuip H, *et al*. Dasatinib reverses cancer-associated fibroblasts (CAFs) from primary lung carcinomas to a phenotype comparable to that of normal fibroblasts. Mol Cancer. 2010;9:168,1-8. DOI: 10.1186/1476-4598-9-168.
70. Du D, Tang X, Li Y, Gao Y, Chen R, Chen Q, *et al*. Senotherapy protects against cisplatin-induced ovarian injury by removing senescent cells and alleviating DNA damage. Oxid Med Cell Longev. 2022;2022:9144644,1-18. DOI: 10.1155/2022/9144644.
71. Gutiérrez-Ortiz JA, González-Ramella O, Solorzano-Ibarra F, Bravo-Cuellar A, Hernández-Flores G, Padilla-Ortega JA, *et al*. Pentoxifylline enhances the effects of doxorubicin and bleomycin on apoptosis, caspase activity, and cell cycle while reducing proliferation and senescence in Hodgkin's disease cell line. Curr Issues Mol Biol. 2025;47(8):593,1-28. DOI: 10.3390/cimb47080593.
72. Bravo-Cuellar A, Ortiz-Lazareno PC, Lerma-Diaz JM, Dominguez-Rodriguez JR, Jave-Suarez LF, Aguilar-Lemarroy A, *et al*. Sensitization of cervix cancer cells to Adriamycin by Pentoxifylline induces an increase in apoptosis and decrease senescence. Mol Cancer. 2010;9:114,1-14. DOI: 10.1186/1476-4598-9-114.
73. El-Far AH, Godugu K, Noreldin AE, Saddiq AA, Almaghrabi OA, Al Jaouni SK, *et al*. Thymoquinone and costunolide induce apoptosis of both proliferative and doxorubicin-induced-senescent colon and breast cancer cells. Integr Cancer Ther. 2021;20:15347354211035450,1-20. DOI: 10.1177/15347354211035450.

Supplementary Materials

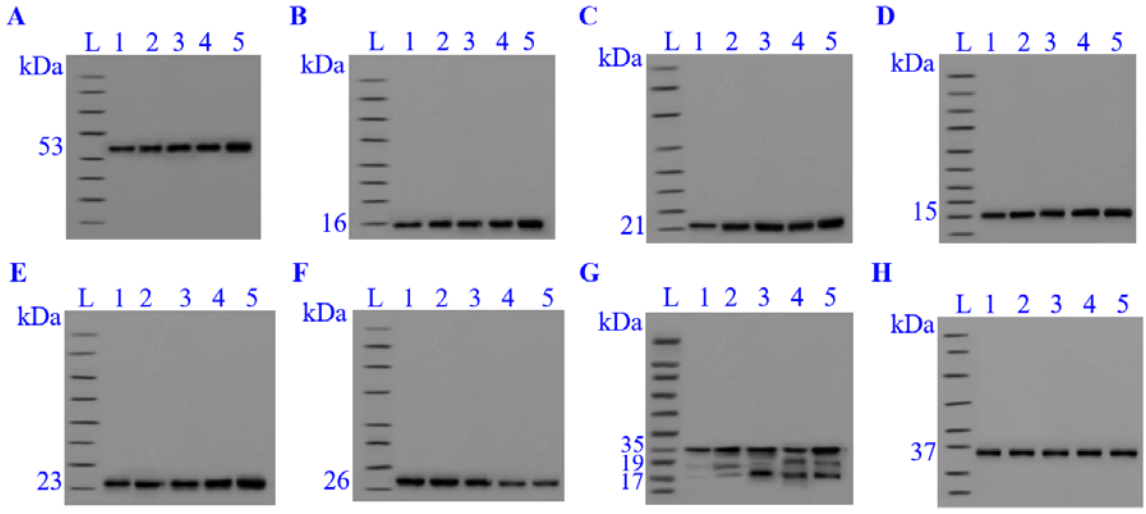

Fig. S1. Western blot analysis of the relative expression of proteins. (A) P53; (B) P16; (C) P21; (D) H2AX; (E) Bax; (F) Bcl2; (G) cleaved caspase 3; (H) GAPDH. L, ladder; lane 1, control; lane 2, 5-FU; lane 3, 5-FU+PTX; lane 4, 5-FU+TQ; lane 5, 5-FU + PTX + TQ; 5-FU, 5-fluorouracil; PTX, pentoxifylline; TQ, thymoquinone.